Structural Consequences of Metallothionein Dimerization: Solution Structure of the Isolated Cd_4-α-Domain and Comparison with the Holoprotein Dimer†

John W. Ejnik,‡ Amalia Muñoz,§ Eugene DeRose,|| C. Frank Shaw III,⊥ and David H. Petering*,||

Northern Michigan University, Marquette, Michigan 49855, Department of Chemistry, University of Wisconsin−Milwaukee, P.O. Box 413, Milwaukee, Wisconsin 53201-0413, Centro Nacional de Biotecnologia (CNB-CSIC), Madrid, Spain, and Department of Chemistry, Eastern Kentucky University, Richmond, Kentucky 40475-3124

Received September 23, 2002; Revised Manuscript Received February 5, 2003

ABSTRACT: The NMR determination of the structure of Cd_7-metallothionein was done previously using a relatively large protein concentration that favors dimer formation. The reactivity of the protein is also affected under this condition. To examine the influence of protein concentration on metallothionein conformation, the isolated Cd_4-α-domain was prepared from rabbit metallothionein-2 (MT 2), and its three-dimensional structure was determined by heteronuclear, ^1H-^{111}Cd, and homonuclear, ^1H-^1H NMR, correlation experiments. The three-dimensional structure was refined using distance and angle constraints derived from these two-dimensional NMR data sets and a distance geometry/simulated annealing protocol. The backbone superposition of the α-domain from rabbit holoprotein Cd_7-MT 2 and the isolated rabbit Cd_4-α was measured at a RMSD of 2.0 Å. Nevertheless, the conformations of the two Cd-thiolate clusters were distinctly different at two of the cadmium centers. In addition, solvent access to the sulfhydryl ligands of the isolated Cd_4-α cluster was 130% larger due to this small change in cluster geometry. To probe whether these differences were an artifact of the structure calculation, the Cd_4-α-domain structure in rabbit Cd_7-MT 2 was redetermined, using the previously defined set of NOEs and the present calculation protocol. All calculations employed the same ionic radius for Cd^{2+} and same cadmium−thiolate bond distance. The newly calculated structure matched the original with an RMSD of 1.24 Å. It is hypothesized that differences in the two α-domain structures result from a perturbation of the holoprotein structure because of head-to-tail dimerization under the conditions of the NMR experiments.

In 1957, the cadmium and zinc binding protein, metallothionein, was discovered by Margoshes and Vallee in equine kidney cortex (*1*). Originally, it was thought to protect cells from heavy metals such as cadmium by tightly sequestering metal ions, thereby rendering them nontoxic (*2*). Because zinc and copper are major constituents of the protein under normal conditions, in the absence of exposure to nonphysiological metal ions, additional roles for MT[1] in zinc and copper metabolism and homeostasis have been proposed and investigated (*3*−*10*).

Mammalian metallothioneins are considered unique small proteins because about one-third of their amino acids are cysteine, which supply sulfhydryl ligands that bind with high affinity a number of metal ions of differing size and chemical properties (*11*, *12*). The 20 cysteines bind seven Cd^{2+} or Zn^{2+} ions or combinations of them in two metal−thiolate clusters (*11*−*14*). This property has focused attention on the role of MT in protection against toxic metal-ion exposure and on possible activities in essential metal-ion metabolism (*2*, *5*, *6*, *15*, *16*). The recognition that there are abundant nucleophilic and oxidizable thiol groups in the MT molecule has led to studies that support functions for the protein in inactivating electrophilic drugs and xenobiotic metabolites as well as oxidant species derived from O_2 (*17*−*20*).

NMR spectroscopy and X-ray diffraction studies have shown that rabbit Cd_7-MT 2 is a dumbbell-shaped molecule (*14*, *21*). The N-terminal, β-domain includes residues 1−29, and the C-terminal, α-domain consists of residues 32−61. They are linked by amino acids 30 and 31. The α-domain binds four bivalent metal ions with five bridging and six terminal cysteine ligands in a boat, chair bicyclo (3,3,1) nonane-like structure (Figure 1a). The β-domain binds three bivalent metal ions with three bridging and six terminal cysteine ligands in a boat, cyclohexane-like structure (Figure 1b). The metal clusters are embedded in the protein's interior by large helical turns of the polypeptide chain.

The reactivity of MT with competing metal ions, ligands, and sulfhydryl reagents is complex because of the presence of the two different protein domains and metal−thiolate clusters (*22*−*28*). To help simplify the analysis of these results, the properties of the C-terminal, α-domain have been examined in comparative studies (*23*, *29*−*32*). In addition, experiments have begun to systematically investigate the roles of cysteine placement and the influence of other residues within domain sequences on cluster formation, stability, and reactivity (*33*).

† This work was supported by NIH Grants ES-04026 and ES-04184 and NSF Grant BIR-9512622.

* To whom correspondence should be addressed. E-mail: petering@uwm.edu. Tel: (414) 229-5853. Fax: (414) 229-5530.

‡ Northern Michigan University.

§ Centro Nacional de Biotecnologia.

|| University of Wisconsin−Milwaukee.

⊥ Eastern Kentucky University.

[1] Abbreviations: α- and β-domains, C- and N-terminal domains of metallothionein; DTNB, 5,5,*N*-dithiobis(2-nitrobenzoate); MT, metallothionein.

10.1021/bi0205956 CCC: $25.00 © 2003 American Chemical Society
Published on Web 06/27/2003

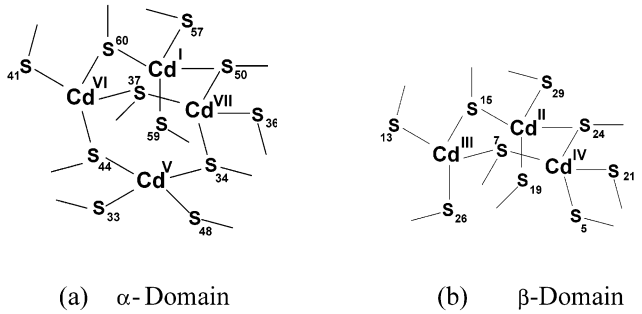

FIGURE 1: Schematic representation of the structures of (a) the four-metal center of the Cd_4-α-domain and (b) the three-metal center of the Cd_3-β-domain.

Head-to-tail, α−β-domain interactions exist among MT molecules in the crystal unit cell used for the X-ray crystallographic determination of the structure of rat Cd_5,-Zn_2-MT 2 (*14*). Dimer formation in solution has been clearly observed using high-resolution gel filtration HPLC to detect monomer and dimer species (*32*). The equilibrium is characterized by a K_d of 3×10^{-4}, consistent with the predominant presence of dimers in millimolar samples of rabbit Cd_7-MT 2 used for the NMR structural analysis (*32*). Such dimeric interactions appear to alter the kinetic reactivity of MT and thus may perturb the structure of the MT molecule (*23*). Since the isolated α-domain cannot form dimers of this type, it is particularly interesting to investigate whether the structure of the isolated α-domain differs in significant ways from that determined in the holoprotein at millimolar concentrations. In this context, the present study reports on the three-dimensional solution structure of the isolated α-domain of rabbit MT 2 and compares it to the α-domain structure in the holoprotein.

MATERIALS AND METHODS

Sample Preparation. Zinc metallothionein was isolated from rabbit livers after injection of animals with 2 mL of 0.15 M $ZnSO_4$ each day for 8 days. Sephadex G-75 and high performance liquid DEAE chromatography were then employed to separate Zn_7-MT and its two isoforms as described previously (*34*). The method of Savas et al. was followed to isolate $^{111}Cd_4$-α from the MT 2 holoprotein (*28*). For ^{1}H NMR experiments, $^{111}Cd_4$-α-domain samples were prepared using a Sephadex G-15 column equilibrated with 20 mM ^{d}Tris/Cl, pH 7.0, in D_2O or 10% D_2O. The $^{111}Cd_4$-α of MT 2 samples were concentrated with a YM-1 Amicon filter membrane. The protein concentration was 3−6 mM in 20 mM ^{d}Tris/Cl, pH 7.0.

NMR Methods. ^{111}Cd and ^{1}H NMR spectra were recorded on a GE GN-500 NMR spectrometer. Spectra were collected using 0.5 mL of 3−6 mM protein solution contained in a 5-mm NMR tube. DQF-COSY, TOCSY, ^{1}H-^{111}Cd HMQC, and NOESY spectra were acquired by routine methods as described in the Supporting Information (*35*−*45*).

Processing NMR Data. The two-dimensional spectra were processed as described in the Supporting Information on a Silicon Graphics Iris 4D/70G computer using FELIX version 2.3 software (Hare Research Inc., Woodinville, WA).

Interproton Distance Restraints. The chemical shifts of all protons in the $^{111}Cd_4$-α-domain were assigned from the COSY and TOCSY spectra and then used to assign NOESY cross-peaks (*46*). A semiquantitative correlation between NOESY cross-peak volume intensities and ^{1}H−^{1}H distance constraints was obtained from a comparison of the NOESY spectra with different mixing times (*47*). The distance constraints were calibrated based on NOE peak volumes of known standard distances within the protein structure that will be referred to as scalar peaks. The scalar NOE peaks used were the β-protons of cysteine 36 and cysteine 44 and the α-protons of glycine 47; a standard distance of 1.8 Å was employed for all three pairs of protons. Distance constraints were classified as strong, medium, or weak corresponding to interproton distance constraints of 1.8−2.7, 1.8−4.0, and 1.8−5.0 Å, respectively (*44*, *48*, *49*).

Torsion Angle Restraints and Stereospecific Assignments. The dihedral angles φ, ψ, χ^1, and χ^2 were determined by measuring the corresponding spin−spin coupling constraints and the intensities of NOE cross-peaks. Relationships between φ and $^3J_{HN\alpha}$, χ^1 and $^3J_{\alpha\beta}$, and χ^2 and $^3J_{Cd,\beta}$, respectively, are well-known (*21*). Constraints on the backbone torsion angles φ and χ^1 were derived from the values of $^3J_{HN\alpha}$ and $^3J_{\alpha\beta}$, respectively, and measured in high-resolution DQF-COSY spectra. Torsion angle constraint ranges for φ were defined as $-120 \pm 40°$ (for $^3J_{HN\alpha} > 8$ Hz) and $-60 \pm 40°$ (for $^3J_{HN\alpha} < 5$ Hz). Torsion angle constraint ranges for χ^1 were set to $-120 \pm 120°$ (for $^3J_{\alpha\beta} > 10$ Hz and $^3J_{\alpha\beta} < 6.5$ Hz) and $-60 \pm 60°$ (for $^3J_{\alpha\beta} < 5$ Hz and $^3J_{\alpha\beta} < 5$ Hz). Constraints on the side-chain cysteine residue torsion angles, χ^2, were derived from the values of $^3J_{Cd,\beta}$, measured in a coupled (^{1}H−^{111}Cd) HMQC spectrum (*21*). Torsion angle constraint ranges for χ^2 were set to $-60 \pm 50°$ (for $^3J_{Cd,\beta a}$ 30−75 Hz and $^3J_{Cd,\beta b}$ 0−30 Hz), $180 \pm 50°$ (for $^3J_{Cd,\beta a}$ and $^3J_{Cd,\beta b}$ 0−30 Hz), and $60 \pm 50°$ (for $^3J_{Cd,\beta a}$ 0−30 Hz and $^3J_{Cd,\beta b}$ 30−75 Hz). Stereospecific assignments for the β-methylene protons were made by analysis of the $^3J_{\alpha\beta}$, measured in the PE-COSY spectrum, and the intraresidue NH-β and α−β NOEs (*21*, *50*−*52*).

Structure Calculations. The cluster unit, comprised of four Cd metal ions and 11 cysteine Sγ atoms, was defined in X-PLOR 3.1 (*21*). Metal−cysteine thiolate connectivities were established from the analysis of ^{1}H−^{111}Cd HMQC data obtained on a ^{111}Cd-enriched α-domain sample. The connectivities were found to be the same as described for holo rabbit MT 2. The Cd^{2+} ions were attached to Sγ of each cysteine residue by distance constraints as described by Wüthrich and co-workers (*21*). All calculations were performed using the program X-PLOR 3.1 and were based on the hybrid distance geometry/dynamical-simulated annealing protocol (*53*). An initial set of structures was generated by randomly selecting values for backbone dihedral angles. From the initial set, 80 structures were generated by adding NOE constraints and dihedral angle constraints. From the annealed structures, only those which had no NOE or dihedral angle violations were accepted.

Recalculation of the Structure of the Cd_4-α-Domain of Rabbit Cd_7-MT 2 and Calculation of Sulfur Atom Solvent Exposure. Structure calculations for the isolated Cd_4-α-domain of metallothionein were carried out using the ab initio simulated annealing/refine protocol (SA), detailed above in this paper, instead of the geometry/simulated annealing protocol (DG) employed in the structure calculation for Cd_7-MT 2 (*54*). Thus, the consistency of both protocols was tested, to ensure that any difference observed between the

Table 1: ^{1}H Chemical Shifts (ppm) for the Isolated $^{111}Cd_4$-α-Domain of MT-2 at pH 7.0 in 20 mM ^{d}Tris-HCl[a]

residue	NH	H^{α}	H^{β}	others
Lys 30		4.38	1.75, 1.84	$C^{\gamma}H_2$ 1.47; $C^{\delta}H_2$ 1.71; $C^{\epsilon}H_2$ 3.01
Lys 31		4.46	1.79, 1.88	$C^{\gamma}H_2$ 1.51; $C^{\delta}H_2$ 1.72; $C^{\epsilon}H_2$ 3.03
Ser 32		4.61	3.75, 4.05	
Cys 33	8.22	4.51	3.25, 3.27	
Cys 34	8.37	5.08	3.55, 3.62	
Ser 35		4.46	3.88, 4.00	
Cys 36	8.54	4.51	2.77, 3.18	
Cys 37	7.20	5.16	3.06	
Pro 38		4.91	2.02, 2.39	$C^{\gamma}H_2$ 1.95, 2.11; $C^{\delta}H_2$ 3.80, 3.88
Pro 39		4.39	1.84, 2.16	$C^{\gamma}H_2$ 2.00, 2.17; $C^{\delta}H_2$ 3.69, 3.91
Gly 40		3.71, 4.03		
Cys 41	7.00	4.08	3.17	
Ala 42	9.38	4.16	1.57	
Lys 43	8.34	4.23	2.09	$C^{\gamma}H_2$ 1.56; $C^{\delta}H_2$ 1.72; $C^{\epsilon}H_2$ 3.06
Cys 44	7.56	4.67	2.62, 3.77	
Ala 45	7.11	4.14	1.52	
Gln 46	8.16	4.58	1.99, 2.43	$C^{\gamma}H_2$ 2.39; NH^{δ} 6.88, 7.56
Gly 47	7.38	3.61, 4.40		
Cys 48		4.36	2.93, 3.00	
Ile 49	7.21	4.73	2.27	$C^{\gamma}H_3$ 1.03; $C^{\gamma}H_2$ 1.06; $C^{\delta}H_3$ 0.96
Cys 50	9.12	4.45	2.65, 3.13	
Lys 51	8.53	4.32	1.84	$C^{\gamma}H_2$ 1.51; $C^{\delta}H_2$ 1.72; $C^{\epsilon}H_2$ 3.03
Gly 52		3.89, 4.09		
Ala 53		4.49	1.46	
Ser 54	8.18	4.64	3.88, 3.92	
Asp 55	8.55	4.40	2.72, 2.77	
Lys 56	7.87	4.73	1.75, 1.82	$C^{\gamma}H_2$ 1.44; $C^{\delta}H_2$ 1.71; $C^{\epsilon}H_2$ 3.04
Cys 57	8.50	5.20	3.60	
Ser 58		4.68	3.91, 3.98	
Cys 59	8.39	4.60	3.24, 3.31	
Cys 60	7.71	4.75	2.69, 2.83	
Ala 61	7.14	4.14	1.42	

[a] The proton chemical shifts were measured at 25 °C. For methylene groups, two chemical shifts are given wherever two resolved signals were observed or where the presence of two degenerated signals had been established unambiguously.

calculated structure of the isolated Cd_4-α-domain and the same domain within the holoprotein was real and not attributable to the differences in protocol used. The solvent exposure of the thiolate groups of the cysteine residues for both structures, Cd_4-α-domain isolated and within the holoprotein, was calculated using MOLMOL 2.6 (Institute für Molekularbiologie und Biophysik, ETH Zürich).

RESULTS

Resonance Assignments. Assignment of the proton resonances of the rabbit $^{111}Cd_4$-α-domain was performed by standard procedures and with information provided by Wagner and Wüthrich (*46*, *49*). The first step involved the association of scalar-coupled resonances with specific spin systems using DQF-COSY and TOCSY experiments and assigning the resonances to amino acid residues (Table 1). COSY, TOCSY, HMQC, and NOESY spectra were all in excellent agreement with proton resonances assigned from spectra of the rabbit $^{113}Cd_4$-α-domain of $^{113}Cd_7$-MT 2 (*46*, *49*, *55*). The cadmium−cysteine connectivities identified by heteronuclear [^{111}Cd, ^{1}H] HMQC were also in agreement with those determined from the $^{113}Cd_4$-α-domain portion of the spectra from $^{113}Cd_7$-MT 2 (*49*, *54*).

Secondary Structure Analysis. NOE assignments were based on definitions of the chemical shifts of protons in COSY and TOCSY spectra. NOE distance contraints were collected from two sets of NOESY spectra, one in H_2O with mixing times of 60, 120, and 250 ms and the other in D_2O with mixing times of 50 and 100 ms. A summary of all the sequential and medium-range NOEs observed in the rabbit $^{111}Cd_4$-α-domain are shown in Figure 1s (Supporting Information). A qualitative analysis of medium-range NOEs indicates that the rabbit $^{111}Cd_4$-α-domain lacks elements of regular secondary structure such as the α-helix and β-sheet.

Table 1s (Supporting Information) lists the $^{3}J_{NH\alpha}$ and $^{3}J_{\alpha\beta}$ values and $NOE_{NH\beta}$ and $NOE_{\alpha\beta}$ intensities that were measured in the rabbit $^{111}Cd_4$-α-domain. The $^{3}J_{\alpha\beta}$ data were extracted from a PE-COSY spectrum. The torsion angle constraints were obtained by procedures described in the Materials and Methods and are listed in this table. The φ angles were constrained in the range of $-120 \pm 40°$ when $^{3}J_{NH\alpha}$ was larger than 8 Hz. Where $^{3}J_{NH\alpha}$ was between 5 and 8 Hz, the torsion angle ranges for φ were not restricted because of averaging of conformations. Finally, Table 1s (Supporting Information) lists the coupling constants for the $^{111}Cd_4$-α-domain that were obtained as described in the Materials and Methods. All the torsion angle constraints were in agreement with the $^{113}Cd_4$-α-domain spectra of $^{113}Cd_7$-MT 2 (*49*, *54*).

Structure Calculations. After simulated annealing calculations, 22 structures were found to have no NOE or dihedral angle violations. The RMSD in angstroms of each residue was calculated with X-PLOR 3.1. From the ensemble of 22 annealed structures, the RMSD of all atoms was calculated to be 1.39 Å. An average structure was calculated from the coordinates of the individual structures. The average structure's energy was minimized by restrained regularization of the mean structure. Table 2 lists the structural statistics and atomic RMS differences from the 22 annealed structures. There was excellent overlap among the 22 annealed structures, resulting in a 1.29 and 0.81 Å RMSD value for the backbone-heavy atoms and metal-cluster atoms of the various structures, respectively. Additionally, all the backbone torsion angles were in acceptable regions of a Ramachandran plot (data not shown).

*Recalculated Cd_4-α-Domain NMR Structure of Rabbit Cd_7-MT 2.*The well-characterized structure of the rabbit liver Cd_7-MT was recalculated using the Wüthrich constraints (NOEs and torsion angles) but our ab initio simulated annealing/refine protocol (*54*). The results obtained were compared with those published, using the geometry/simulated annealing protocol (*54*). The RMSD for both structures was calculated using the molecular program SYBYL. When the structure of the α-domain within Cd_7-MT was recalculated as described, RMSD values of 1.24 and 1.59 Å for the backbone and the whole domains (backbone and side-chain groups), respectively, were within the error limits for the RMSD calculated for the 10 NMR structures of 1.7 ± 0.2 Å reported by Wüthrich et al. (*54*). This finding supported the conclusion that any differences in structure observed between the isolated α-domain and the α-domain in the holoprotein were not an artifact of the SA protocol.

The α-domain structure of Cd_7-MT was based on 23 sequential backbone contraints, 11 medium and long-range backbone constraints, 46 interresidue NOE constraints with side-chain protons, and 28 angle constraints (*54*). The structure calculation of the isolated α-domain utilized 19 sequential backbone contraints, eight medium and long-range backbone constraints, 46 interresidue NOE constraints with side-chain protons, and 29 angle constraints. The quantitative

Table 2: Structural Statistics and Atomic RMS Differences for the Calculated NMR Structures of the Isolated $^{111}Cd_4$-α-Domain of Metallothionein-2[a]

A. Structural Statistics	⟨SA⟩	$(SA)_r$
RMS deviations from exptl distance restraints (Å)[b]		
all (163)	0.058 ± 0.005	0.056
interresidue sequential ($(i-j)=2$)	0.058 ± 0.007	0.052
interresidue sequential ($(i-j)>2$)	0.065 ± 0.013	0.051
intraresidue	0.063 ± 0.006	0.056
RMS deviations from exptl dihedral restraints (deg)	0.610 ± 0.241	2.734
RMS deviations from idealized covalent geometry used within X-PLOR		
bonds (D)	0.004 ± 0.0002	0.004
angles (deg)	0.637 ± 0.033	0.761
impropers (deg)	0.515 ± 0.024	0.574
selected X-PLOR energies (kcal/mol)[c]		
E_{bond}	5.97 ± 0.76	6.18
E_{angle}	51.24 ± 4.86	65.42
$E_{improper}$	7.69 ± 0.72	9.52
E_{NOE}	35.98 ± 5.97	39.67
E_{cdhi}	0.71 ± 0.45	6.83
E_{repel}	8.23 ± 2.49	53.32
E_{total}	109.91 ± 12.3	180.54

B. Atomic RMS Differences (D)	⟨SA⟩ vs (SA)
all atoms (33−61)	1.39 ± 0.17
backbone-heavy atoms of all residues (31−61)	1.29 ± 0.20
backbone-heavy atoms of residues 33−61	1.09 ± 0.16
metal-cluster atoms (4 Cd^{2+} and 11 S^{γ})	0.81 ± 0.07

[a] The notation of the NMR structures is as follows: ⟨SA⟩ represents the final 22 annealed structures, (SA) is the mean structure obtained by averaging the coordinates of the individual ⟨SA⟩ structures best fit to each other, and $(SA)_r$ is the restrained minimized mean structure obtained by restrained regularization of the mean structure, (SA) (*53*). [b] None of the structures exhibited NOE-derived distance violations greater than 0.5 Å or backbone dihedral angle violations greater than 5 °C. [c] Energies were calculated by X-PLOR using a square well potential for the NOE term (100 kcal/mol Å^2) and a square well quadratic energy function for the torsional potential (200 kcal/mol rad^2).

similarity in the information used to define each structure also argues that they can be compared for differences in conformation.

Comparison of the Structures of Isolated Cd_4-α-Domain and the Cd_4-α-Domain in Cd_7-MT. Comparison of the structures of the α-domain in the isolated peptide and the entire protein showed that the ^{111}cadmium−cysteine *β*-proton connectivities are identical in the two structures. As a consequence, the overall peptide backbone fold about the central Cd_4S_{11} cluster must be the same. The proton ^{1}H chemical shifts for residues derived from the two α-domains are also in agreement in terms of assignment but consistently differ from one another, indicative of differences in the two structures (*54*). Superposition of the final backbone structures derived from the constraints of the cadmium−cysteine connectivities and the NOE information show that they share very similar conformations with an RMSD of 2.0 Å (Figure 2). They differed most clearly in their N-terminal conformations where the first two to three residues of the peptide did not exhibit much structural organization. This was anticipated because these residues attached to the linker, and the *β*-domain in the Cd_7-MT would likely display a different orientation.

An examination of the space-filled models of the two structures reveals, first, that the α-domain of the holoprotein is more compact (Figure 3). Second, the hydrogen bond interactions, exclusive of NH−S bonding, that are derived

FIGURE 2: Superposition of the backbone structures of the isolated Cd_4-α-domain (red) and the domain within the holoprotein, Cd_7-MT (yellow). N-terminus, lower left.

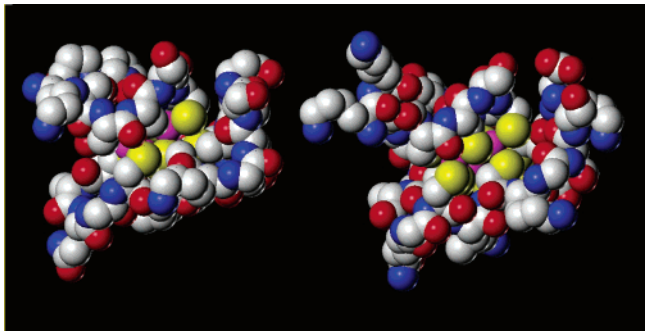

FIGURE 3: Comparison of the space-filled representations of the isolated Cd_4-α-domain (right) and the domain within the holoprotein, Cd_7-MT (left).

Table 3: Sulfur−Cadmium−Sulfur Bond Angles (deg) for Each Cd Center of Isolated Cd_4-α and Cd_7-MT

	isolated Cd_4-α[a]		Cd_4-α domain of Cd_7-MT[b]	
	d (Å)	$\angle_{S-Cd-S}$	*d* (Å)	$\angle_{S-Cd-S}$
Cd^{I}		S_{50}−Cd−S_{57}: 108.4		S_{50}−Cd−S_{57}: 108.6
	S_{50}: 2.46	S_{50}−Cd−S_{59}: 104.4	S_{50}: 2.53	S_{50}−Cd−S_{59}: 111.4
	S_{57}: 2.45	S_{50}−Cd−S_{60}: 112.3	S_{57}: 2.50	S_{50}−Cd−S_{60}: 95.1
	S_{59}: 2.59	S_{57}−Cd−S_{59}: 113.6	S_{59}: 2.47	S_{57}−Cd−S_{59}: 106.6
	S_{60}: 2.56	S_{57}−Cd−S_{60}: 99.0	S_{60}: 2.64	S_{57}−Cd−S_{60}: 107.2
		S_{59}−Cd−S_{60}: 119.0		S_{59}−Cd−S_{60}: 126.8
Cd^{V}		S_{33}−Cd−S_{34}: 113.0		S_{33}−Cd−S_{34}: 104.3
	S_{33}: 2.58	S_{33}−Cd−S_{44}: 106.3	S_{33}: 2.52	S_{33}−Cd−S_{44}: 112.8
	S_{34}: 2.48	S_{33}−Cd−S_{48}: 104.2	S_{34}: 2.63	S_{33}−Cd−S_{48}: 123.8
	S_{44}: 2.58	S_{34}−Cd−S_{44}: 112.1	S_{44}: 2.53	S_{34}−Cd−S_{44}: 107.3
	S_{48}: 2.55	S_{34}−Cd−S_{48}: 105.0	S_{48}: 2.50	S_{34}−Cd−S_{48}: 104.3
		S_{44}−Cd−S_{48}: 106.3		S_{44}−Cd−S_{48}: 103.1
Cd^{VI}		S_{37}−Cd−S_{41}: 110.8		S_{37}−Cd−S_{41}: 120.2
	S_{37}: 2.56	S_{37}−Cd−S_{44}: 115.8	S_{37}: 2.72	S_{37}−Cd−S_{44}: 115.1
	S_{41}: 2.54	S_{37}−Cd−S_{60}: 103.6	S_{41}: 2.48	S_{37}−Cd−S_{60}: 90.5
	S_{44}: 2.59	S_{41}−Cd−S_{44}: 119.2	S_{44}: 2.64	S_{41}−Cd−S_{44}: 92.2
	S_{60}: 2.57	S_{41}−Cd−S_{60}: 103.9	S_{60}: 2.49	S_{41}−Cd−S_{60}: 135.2
		S_{44}−Cd−S_{60}: 100.9		S_{44}−Cd−S_{60}: 103.8
Cd^{VII}		S_{34}−Cd−S_{36}: 119.8		S_{34}−Cd−S_{36}: 109.3
	S_{34}: 2.49	S_{34}−Cd−S_{37}: 109.3	S_{34}: 2.47	S_{34}−Cd−S_{37}: 104.6
	S_{36}: 2.40	S_{34}−Cd−S_{50}: 103.1	S_{36}: 2.44	S_{34}−Cd−S_{50}: 96.3
	S_{37}: 2.50	S_{36}−Cd−S_{37}: 111.0	S_{37}: 2.44	S_{36}−Cd−S_{37}: 133.62
	S_{50}: 2.49	S_{36}−Cd−S_{50}: 100.7	S_{50}: 2.70	S_{36}−Cd−S_{50}: 110.4
		S_{37}−Cd−S_{50}: 112.3		S_{37}−Cd−S_{50}: 96.1

[a] This paper. [b] Ref *54*.

from examining the two average calculated structures are different (Table 2s). Third, whereas the S−Cd−S bond angles of each Cd center in the isolated α-domain generally approximate ideal tetrahedral geometry of 108° (Table 3), there are a number of large distortions in the α-domain of the holoprotein, most of which are found among the bond

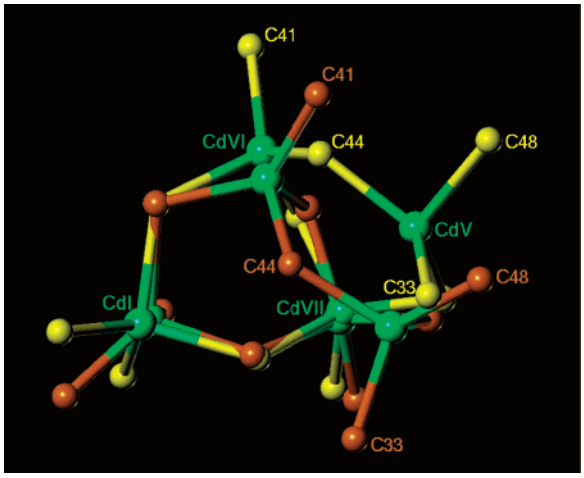

FIGURE 4: Superposition of the metal centers of the isolated Cd_4-α-domain (orange) and the domain within the holoprotein, Cd_7-MT (yellow).

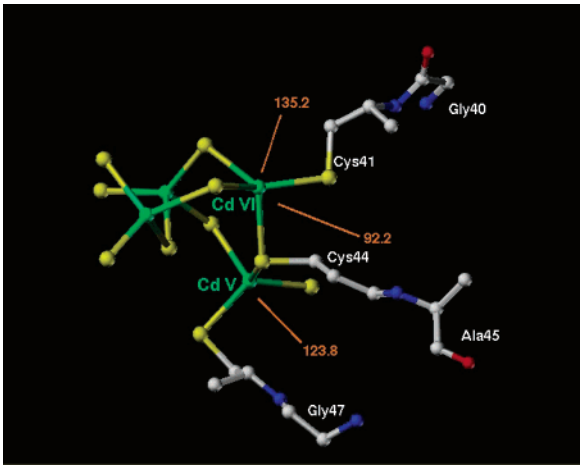

FIGURE 5: Possible dimer interface of Cd_4-α-domain based on X-ray structural information and a partial Cd-thiolate cluster (*14*).

angles about Cd^{VI}. As indicated in the Materials and Methods, the distance and angle constraints applied in both calculations were identical. Therefore, the differences in bond angles appear to result from structural differences between the domains. Fourth, the sulfur atoms of the cluster of Cd_4-α are more exposed to solvent as shown by a comparison of the solvent-exposed surface of the sulfur atoms in the two structures (Tables 4 and 5). As a result, the present structure opens up the cluster to the solvent such that five thiolates from cysteines 37, 41, 48, 57, and 59 have a surface exposure greater than 5 $Å^2$. In contrast, only sulfhydryl groups from residues 33 and 59 display appreciable solvent access in the α-domain of the Cd_7-MT structure. Figure 4 shows an overlay of the structures of each cadmium−thiolate cluster. Cadmium atoms I, VI, and VII and their bridging sulfurs from Cys 37, 50, and 60 reasonably overlap with one another. However, the distorted ligand geometry around Cd^{VI}, particularly involving the thiolate of Cys44 that bridges between Cd^{VI} and Cd^{V}, leads to an obvious difference in the position of Cd^{V} in the two structures; Cys44 binds to Cys 48, one of the residues that contributes a highly exposed thiolate group in the isolated α-domain. To test the importance of the bond angle distortion about Cd^{VI} in Cd_7-MT, the geometry of the Cd−S bonds of Cd^{VI} in Cd_7-MT were changed to those of Cd^{VI} in the isolated Cd_4-α, employing the molecular modeling program SYBYL 6.5. Then, after energy minimization using the Tripos force-field and the Gasteiger−Hückel algorithm for the charges, the overall conformations of both clusters converged. Furthermore, the conformation of the entire domains closely resembled one another, especially, when the crevice opened up providing more solvent accessibility to the sulfur atoms.

DISCUSSION

The structure of rabbit Cd_7-MT 2 was previously determined by Wüthrich and co-workers using NMR techniques (*46*, *54*). Later, Stout and co-workers used X-ray crystallographic methods to obtain a similarly folded structure for (Cd_5,Zn_2)-MT 2 from rat liver (*14*, *56*). Since no interdomain constraints between the α- and β-domains were detected in either study, the structure of Cd_4-α of MT 2 was considered an independent part of the holoprotein. Nevertheless, in the unit cell of crystallized (Cd_5,Zn_2)-MT 2, metallothionein molecules establish a head-to-tail orientation of adjacent α- and β-domains that suggests intermolecular interactions (*14*). Subsequent experiments using calibrated gel filtration HPLC clearly demonstrated under solution conditions similar to those used in this study that Cd_7-MT dimerizes with an equilibrium constant of about 3×10^4 (*32*). Accordingly, at the millimolar concentrations of protein used in the NMR work, rabbit Cd_7-MT exists as a dimer in solution (*32*, *46*, *54*). Therefore, the calculated structure may reflect features of the dimer that have not been previously recognized.

The reactivity of rabbit liver Cd_7-MT with EDTA varies inversely with protein concentration (*23*). In another recent study, the rate constant for the metal-ion exchange reaction between Zn_7-MT and cadmium−carbonic anhydrase also varied inversely with MT protein concentration over the range where the monomer/dimer ratio changes significantly (*57*). Both findings indicate that there are functional consequences of dimer formation that may relate to conformational changes resulting from α−β-domain interactions.

It is hypothesized that such bimolecular reactions are governed by the access of these reagents to thiolate ligands where competition for binding to Cd or Zn takes place. Tables 4 and 5 list the solvent accessibility of each sulfur atom of Cd_4-α in the isolated structure and in the holoprotein and show that the individual α-domain has more than twice the solvent-accessible surface area of its thiolate groups as does the α-domain from the holoprotein (50 vs 22 $Å^2$). In particular, the prominent crevice, a major site of solvent exposure for the sulfhydryl groups in the α-domain, is much more open in the isolated structure (Figure 3). With an aggregate sulfur atom exposure of 23.5 $Å^2$ (Cys 36, 37, 41, 57), it displays more than two times greater accessible surface area of its thiolate groups than in the holoprotein (10.0 $Å^2$). Furthermore, the sulfur atom of Cys 48 bound to Cd^{V} has 9.0 $Å^2$ exposure in Cd_4-α and none in Cd_7-MT.

The basis for the difference in thiolate surface area of these structures can be assigned to distinct positioning of cysteine side-chain methylene and backbone (-CH(NH)CO) moieties with respect to the Cd_4S_{11} clusters in the two domains (Tables 4 and 5). Comparison of the cadmium−thiolate clusters with only the cysteinyl groups attached shows that the solvent exposure of the sulfur atoms in the isolated domain is much larger than that of the holoprotein α-domain (120 vs 68 $Å^2$) (Figure 5). Table 5 shows the additional contribution of the

Table 4: Survey of the Changes in Surface Solvent Exposure (Å^2) of the Sulfur Atoms of Cysteine Residues in the Isolated Cd_4-α-Domain of MT Calculated Based on a 1.4 Å Probe Sphere

				Cd_4Cys_{11}-bb plus sequential side-chain addition[a,b]													
Cys[c]	Cd_4S_{11}[d]	Cd_4Cys_{11}[e]	Cd_4Cys_{11}-bb[f]	K31	S32	S35	P38	A42	K43	Q46	G47	I49	K51	A53	D55	K56	S58	domain
33	77	8.0	5.5	–	–	–	–	–	–	–	–	–	4.5	–	–	–	–	4.5
34	48	6.0	4.5	4.0	–	3.5	–	–	–	–	–	–	–	–	–	–	–	3.5
36	68	6.0	4.0	–	–	–	–	–	–	–	–	–	–	–	3.5	3.0	–	3.0
37	35	7.0	7.0	–	–	–	6.0	–	–	–	–	–	–	–	–	–	–	6.0
41	80	20.0	14.0	–	–	–	12.5	11.5	6.0	–	–	–	–	–	–	–	–	6.0
44	38	1.5	0.0	–	–	–	–	–	–	–	–	–	–	–	–	–	–	0.0
48	74	24.9	14.5	12.0	11.5	–	–	–	–	10.5	9.0	–	–	–	–	–	–	9.0
50	32	5.5	1.5	–	–	–	–	–	–	–	–	–	0.0	–	–	–	–	0.0
57	68	9.5	9.0	–	–	–	–	–	–	–	–	–	–	–	–	–	8.5	8.5
59	83	23.9	19.5	–	–	–	–	–	–	–	–	10.5	–	9.5	–	–	–	9.5
60	35	7.5	3.5	–	–	–	–	–	0.0	–	–	–	–	–	–	–	–	0.0
total	638	119.8	83.0															50.0

[a] Dash indicates that the solvent exposure of the cysteine sulfur remains constant upon inclusion of the new side chain. [b] bb, domain backbone, the polypeptide chain minus the variable side chains. [c] Number of cysteine residue. [d] Surface area of sulfur atoms in Cd_4S_{11} cluster core minus all other atoms of the domain. [e] Surface area of sulfur atoms in Cd_4Cys_{11}, the cluster core, plus the rest of the backbone and side chain of cysteine, $-CH_2CH(NH-)CO-$. [f] Surface area of sulfur atoms in Cd_4Cys_{11} plus the rest of the polypeptide backbone minus the noncysteine, variable side chains.

Table 5: Survey of the Changes in Surface Solvent Exposure (Å^2) of the Sulfur Atoms of Cysteine Residues (r) in the α-Domain of Cd_7-MT Calculated Based on a 1.4 Å Probe Sphere[a]

				Cd_4Cys_{11}-bb plus sequential side-chain addition										
Cys	Cd_4S_{11}	Cd_4Cys_{11}	Cd_4Cys_{11}-bb	S32	S35	P38	P39	K43	I49	K51	A53	S54	D55	S58	domain
33	78	19.0	12.0	8.0	–	6.0	5.5	–	–	–	–	–	–	–	5.5
34	38	0.0	0.0	–	–	–	–	–	–	–	–	–	–	–	0.0
36	75	12.5	7.0	–	6.0	–	–	–	–	–	5.5	4.0	3.5	–	3.5
37	39	3.0	3.0	–	–	–	–	–	–	–	–	–	–	–	3.0
41	76	6.0	3.5	–	–	2.0	–	–	–	–	–	–	–	–	2.0
44	29	2.5	1.0	–	–	–	–	0.0	–	–	–	–	–	–	0.0
48	68	0.5	0.5	–	–	–	–	–	–	0.0	–	–	–	–	0.0
50	11	0.0	0.0	–	–	–	–	–	–	–	–	–	–	–	0.0
57	56	2.0	1.5	–	–	–	–	–	–	–	–	–	–	–	1.5
59	82	13.0	11.0	–	–	–	–	–	9.5	8.0	–	–	–	6.5	6.5
60	48	9.0	0.0	–	–	–	–	–	–	–	–	–	–	–	0.0
total	600	67.5	39.5												22.0

[a] Abbreviations are as in Table 4.

rest of the backbone (37 vs 28 Å^2) to burying the cluster sulfur atoms and indicates that side chains reduce surface exposure in the isolated domain and holoprotein by only 33 and 18 Å^2, respectively. Indeed, in the isolated α-domain, only side chains of residues 43 and 49 shield more than 2.5 Å^2 (11.5 and 9 Å^2, respectively) of the sulfur atom surface, and 12 others provide smaller steric barriers to the solvent. Similarly, in the α-domain of Cd_7-MT, only the side-chain group of K32 reduces solvent exposure by more than 2.5 Å^2; 10 others make smaller contributions.

Table 3s (Supporting Information) shows a comparison of the total sulfur solvent exposure in the Cd_4-α-domain structures of the four Cd_7-MT NMR structures in the Protein Data Bank. Solvent-accessible surface of the sulfurs ranges from 22 to 50 Å^2. The other domains have substantially less accessible surface than the 50 Å^2 for the isolated Cd_4-α-domain. The similarity in sulfur surface areas among the four holoprotein structures suggests that they may display depressed reactivity because of dimerization under NMR conditions in comparison with the same structures examined in the monomeric state at micromolar concentrations.

The analysis based in Tables 4 and 5 as well as the summary information in Table 3s (Supporting Information) implies that the conformations of cysteinyl residues about the Cd_4-α clusters in the holoprotein and isolated domain structures are different and are primary determinants of the sulfur atom exposure in the complete domains. Noncysteinyl residues play only a secondary role in establishing the solvent-accessible surface of the clusters. Such conclusions are consistent with Table 3, which summarizes the cadmium−thiolate geometries of each Cd_4S_{11} cluster. Generally, the S−Cd−S bond angles of the isolated α-domain approximate 108°, whereas there are a number of large excursions from the ideal tetrahedral geometry in the α-domain of the holoprotein. Specifically, four of the six bond angles of Cd^{VI} in the holoprotein deviate substantially from tetrahedral geometry. When the clusters are overlaid, as in Figure 4, such that the two Cd_3S_3 boat conformations involving cadmiums I, IV, and VII largely overlap, the distorted coordination of thiolate groups by Cd^{VI} displaces the position of Cd^{V} and its bound thiolate groups in the holoprotein structure through a shift in position of their common bridging sulfhydryl ligand from Cys 44. Referring to Tables 4 and 5, it is apparent that the solvent exposure of six of 11 sulfur atoms differs in the two structures and that this difference is expanded to nine as the structures are stripped down to their clusters and cysteinyl methylene and backbone atoms. Thus, even though the fold of the backbone is very similar in the two structures, subtle differences are magnified into a large difference in solvent access of the cluster thiolates.

Evidently, a consequence of this conformational change is that the sulfur atom of Cys 48 assumes a different spatial orientation in the two structures, displaying 9.0 Å^2 surface area in the isolated Cd_4-α-domain and 0.0 Å^2 in Cd_7-MT. The lack of surface exposure of the Cys 48 sulfur in the latter structure had made it difficult to explain the preferential alkylation of this site by bulky alkylating agents (*58*−*61*). In contrast, if the isolated Cd_4-α-domain represents the structure of the α-domain in Cd_7-MT at low concentration, then the large exposed surface of the Cys 48 thiolate is a favorable target for reaction.

The clear-cut difference in crevice conformation and sulfur atom exposure to solvent in the two structures provides the basis for a structural hypothesis to explain the protein concentration-dependent change in reactivity of the holoprotein with EDTA (*23*). According to the proposed mechanism of reaction, the Cd_4-α-domain undergoes a biphasic reaction with EDTA with one Cd ion reacting in a faster, EDTA independent step and the other three in a slower process that involves initial binding of EDTA prior to complete ligand substitution. It is hypothesized that the first reaction involves Cd^V, which is linked to the solvent through the thiolate groups of Cys33 and 48.

$$Cd_4\text{-}\alpha + EDTA \rightarrow Cd_3\text{-}\alpha + CdEDTA \qquad (1)$$

$$Cd_3\text{-}\alpha + EDTA \overset{K_d}{\rightleftharpoons} EDTA\text{-}Cd_3\text{-}\alpha \overset{k}{\rightarrow} \alpha + 3Cd\text{-}EDTA \qquad (2)$$

Once this reaction has occurred, the residual Cd_3S_9 cluster undergoes a concerted reaction through the binding mechanism that probably is initiated in the crevice involving thiolates from Cys 36, 37, 41, and 57. According to kinetic, spectrophotometric, and mass spectral evidence, an intermediate EDTA-cluster adduct forms in which some thiolate ligands have been replaced by ones from EDTA (eq 1) (*23*, *62*).

The conformational change of the Cd_4-α-domain in Cd_7-MT buries the sulfur atom of Cys 48 and greatly diminishes the surface exposure of thiolates in the crevice (Cys 36, 37, 41 and 57). Both effects are expected to limit the reactivity of the domain with EDTA based on the proposed mechanism. In particular, steric restrictions could limit the rate of eq 2 either by inhibiting the extent of initial adduct formation or the rate at which other ligands of EDTA can complete the attack on the cluster to release Cd^{2+} as Cd-EDTA.

Residues from the α-domain that participate in intermolecular contacts in the crystal structure include G40, A42, S45, Q46, and G47 (*14*). Generally, these are invariant among MT sequences, yet amino acids 40−47 do not comprise a part of the major crevice of the α-domain. So, it cannot be argued that the large reduction in rate of reaction of EDTA with the α-domain of Cd_7-MT at millimolar concentrations of protein is due to direct intermolecular interactions at or near the crevice that cause steric hindrance. Instead, other structural interactions between the α- and the *β*-domains might induce a small reorganization of the cluster that may modulate the size of the crevice and reduce its access to reactive molecules in the solvent. Possibly, dimer interactions involving residues in the region of residues 40−47 contribute to the distortion of Cd−S bonding about Cd^{VI} (Figure 5). For example, cysteine 41 that binds to Cd^{VI} assumes a distorted geometry in Cd_7-MT (Table 3), causing its side-chain methylene to cover both its own sulfhydryl group and also reduce the solvent exposure of the sulfur atom of cysteine 34. The perturbation of cysteine 41 might be due to dimer interactions that alter the conformation of glycine 40 and alanine 42 and in the process change the orientation of the intervening residue. Similarly, the change in position of the bridging sulfur atom of Cys 44 in the holoprotein may be attributed to a conformational perturbation of neighboring side chains, Ala 45 and Gly 47, that are involved in the putative dimer interface.

The difference in thiolate solvent exposure in the two structures may serve as a structural model to help rationalize the fact that a number of rate laws for reaction of reagents with metallothionein contain first-order terms that are independent of reagent concentration. For example, the rate law for the reaction of Cd_7-MT with DTNB is

$$k_{obs} = k_\alpha + k_\alpha'[DTNB] + k_\beta + k_\beta'[DTNB] \qquad (3)$$

Besides second-order terms for the bimolecular reaction of DTNB with each cluster, there are also two first-order terms associated with their reactions with DTNB (*29*, *30*). The first-order processes have been described as ill-defined unimolecular events in the two domains that are rate limiting in the reaction of the clusters with DTNB. Recognizing in the present structural work that a small reorganization of the cluster can significantly alter its solvent accessibility, one may hypothesize that a rate-limiting conformational change, k_α, occurs in which the cluster undergoes a small conformational change to open up the crevice to a subsequent rapid attack by DTNB (eq 4).

$$\alpha\text{-domain} \overset{K_\alpha}{\rightleftharpoons} \alpha\text{-domain}' \overset{DTNB}{\rightleftharpoons} \text{products} \qquad (4)$$

The results presented here enlarge the understanding of the structural basis of the chemical reactivity and in vivo function of metallothionein. At low micromolar concentrations of zinc metallothionein as found in Ehrlich cells in the absence of induction of MT synthesis, the native protein may be active in intracellular zinc distribution as previously hypothesized (*63*, *64*). Consistent with this possibility, the α-domain cluster is comparatively accessible to agents in the solvent and is, thus, relatively reactive at such concentrations (*63*). Upon induction of MT by exposure to Cd^{2+}, the concentration of Cd,Zn-MT may approach millimolar concentrations. A role of the protein in the presence of Cd^{2+} is to sequester the toxic metal ion in an innocuous form so that it does not compromise normal cell functions (*65*). Although the high affinity of the cadmium−thiolate clusters for Cd^{2+} favors its binding to the thionein protein, it has been suggested that other agents may be able to mobilize Cd^{2+} from the protein, leading to toxicity. For example, NO has been reported to displace Cd^{2+} both in vitro and in cells (*66*). In circumstances of large MT concentration, the dimerization property may be an important secondary mechanism that limits MT reactivity and release of Cd^{2+}.

SUPPORTING INFORMATION AVAILABLE

Routine details about NMR methods as well as three tables (1s−3s) and a figure (1s). Table 1s, spin−spin couplings (Hz) and NOE intensities in rabbit MT-2 α-domain; Table 2s, hydrogen bonds in the isolated Cd_4-α-domain and Cd_4-

α-domain of Cd_7-MT; Table 3s, information on the comparative solvent accessibility of the sulfurs in the Cd_4-α-domains of MT NMR structures; and Figure 1s, a schematic representation of the sequential and medium range NOEs observed in the isolated $^{113}Cd_4$-α-domain. This material is available free of charge via the Internet at http://pubs.acs.org.

REFERENCES

1. Margoshes, M., and Vallee, D. L. (1957) *J. Am. Chem. Soc. 79*, 4813−4814.
2. Hamer, D. H. (1986) *Annu. Rev. Biochem. 55*, 913−951.
3. Bremner, I. (1993) in *Metallothionein III: Biological Roles and Medical Implications* (Suzuki, K. T., Imura, N., and Kimura, M., Eds.) pp 112−124, Birkhäuser Verlag, Basel, Switzerland.
4. Winge, D. R., and Dameron, C. T. (1993) in *Metallothionein III: Biological Roles and Medical Implications* (Suzuki, K. T., Imura, N., and Kimura, M., Eds.) pp 381−397, Birkhäuser Verlag, Basel, Switzerland.
5. Udom, A., and Brady, F. O. (1980) *Biochem. J. 187*, 329−335.
6. Li, T.-Y., Kraker, A. J., Shaw, C. F., III, and Petering, D. H. (1980) *Proc. Natl. Acad. Sci. U.S.A. 77*, 6337−6338.
7. Jiang, L.-J., Maret, W., and Vallee, B. L. (1998) *Proc. Natl. Acad. Sci. U.S.A. 95*, 3483−3488.
8. Jacob, C., Maret, W., and Vallee, B. L. (1998) *Proc. Natl. Acad. Sci. U.S.A. 95*, 3489−3494.
9. Maret, W. (1994) *Proc. Natl. Acad. Sci. U.S.A. 91*, 237−241.
10. Maret, W., and Vallee, B. L. (1998) *Proc. Natl. Acad. Sci. U.S.A. 95*, 3478−3482.
11. Vašák, M., and Kägi, J. H. R. (1983) *Met. Ions Biol. Syst. 15*, 213−273.
12. Vašák, M., and Kägi, J. H. R. (1981) *Proc. Natl. Acad. Sci. U.S.A. 78*, 6709−6713.
13. Otvos, J. D., and Armitage, I. M. (1980) *Proc. Natl. Acad. Sci. U.S.A. 77*, 7094−7098.
14. Robbins, A. H., McRee, D. E., Williamson, M., Collett, S. A., Xuong, N. H., Furey, W. F., Wang, B. C., and Stout, C. D. (1991) *J. Mol. Biol. 221*, 1269−1293.
15. Bremner, I. (1993) in *Metallothionein III: Biological Roles and Medical Implications* (Suzuki, K. T., Imura, N., and Kimura, M., Eds.) pp 112−124, Birkhäuser Verlag, Basel, Switzerland.
16. Winge, D. R., and Dameron, C. T. (1993) in *Metallothionein III: Biological Roles and Medical Implications* (Suzuki, K. T., Imura, N., and Kimura, M., Eds.) pp 381−397, Birkhäuser Verlag, Basel, Switzerland.
17. Thornally, P. J., and Vašák, M. (1985) *Biochim. Biophys. Acta 827*, 36−44.
18. Abel, J., and De Ruiter, N. (1989) *Toxicol. Lett. 47*, 191−196.
19. Endersen, L., Bakka, A., and Rugstad, H. A. (1983) *Cancer Res. 43*, 2918−2926.
20. Cagen, S. Z., and Klaassen, C. D. (1979) *Toxicol. Appl. Pharmacol. 51*, 107−116.
21. Braun, W., Wagner, G., Wörgötter, E., Vašák, M., Kägi, J. H., and Wüthrich, K. K. (1986) *J. Mol. Biol. 187*, 125−129.
22. Shaw, C. F., III, He, L., Muñoz, A., Savas, M. M., Chi, S., Fink, C. L., Gan, T., and Petering, D. H. (1997) *J. Biol. Inorg. Chem. 2*, 65−73.
23. Gan, T., Muñoz, A., Shaw, C. F., III, and Petering, D. H. (1995) *J. Biol. Chem. 270*, 5339−5345.
24. Otvos, J. D., Petering, D. H., and Shaw, C. F., III (1989) *Comments Inorg. Chem. 9*, 1−35.
25. Zhu, Z., Petering, D. H., and Shaw, C. F., III (1995) *Inorg. Chem. 34*, 4477−4483.
26. Li, Y.-T., Minkel, D. T., Shaw, C. F., III, and Petering, D. H. (1981) *Biochem. J. 193*, 441−446.
27. Schmitz, G., Minkel, D. T., Gingrich, D., and Shaw, C. F., III (1980) *J. Inorg. Biochem. 12*, 293−306.
28. Shaw, C. F., III, Laib, J. E., Savas, M. M., and Petering, D. H. (1990) *Inorg. Chem. 29*, 403−408.
29. Savas, M. M., Petering, D. H., Shaw, C. F., III (1991) *Inorg. Chem. 30*, 581−583.
30. Muñoz, A., Petering, D. H., and Shaw, C. F., III (1999) *Inorg. Chem. 38*, 2655−2659.
31. Bernhard, W. R., Vašák, M., and Kägi, J. H. R. (1986) *Biochemistry 25*, 1975−1980.
32. Otvos, J. D., Liu, X., Li, H., Shen, G., and Basti, M. (1993) in *Metallothionein III: Biological Roles and Medical Implications* (Suzuki, K. T., Imura, N., and Kimura, M., Eds.) pp 57−74, Birkhäuser Verlag, Basel, Switzerland.
33. Muñoz, A., Petering, D. H., and Shaw, C. F., III (2000) *Inorg. Chem. 39*, 6114−6123.
34. Minkel, D. T., Poulsen, K., Wielgus, S., Shaw, C. F., III, and Petering, D. H. (1980) *Biochem. J. 191*, 475−485.
35. Rance, M., Sorensen, O. W., Bodenhausen, G., Wagner, G., Ernst, R. R., and Wüthrich, K. (1983) *Biochem. Biophys. Res. Commun. 117*, 479−485.
36. Marion, D., Ikura, M., Tschudin, R., and Bax, A. (1989) *J. Magn. Reson. 85*, 393−339.
37. Shaka, A. J., Barker, P. B., and Freeman, R. (1985) *J. Magn. Reson. 64*, 547−552.
38. Bax, A., and Lerner, L. (1988) *J. Magn. Reson. 79*, 429−438.
39. Mueller, L. (1987) *J. Magn. Reson 72*, 191−196.
40. Braunschweiler, L., and Ernst, R. R. (1983) *J. Magn. Reson. 53*, 521−528.
41. Bax, A., and Davis, D. G. (1985) *J. Magn. Reson. 65*, 335−360.
42. Blake P. R., Park, J. B., Bryant, F. O., Aono, S., Magnuson, J. K., Eccleston, E., Howard, J. B., Summers, M. F., and Adams, M. W. (1991) *Biochemistry 30*, 10885−10895.
43. Frey, M. H. (1985) *J. Am. Chem. Soc. 107*, 6847−6851.
44. Jeener, J. J., Meier, B. H., Bachmann, P., and Ernst, R. R. (1979) *J. Chem. Phys. 7*, 4556−4553.
45. States, D. J., Haberkorn, R. A., and Ruben, D. J. (1982) *J. Magn. Reson. 48*, 286−292.
46. Wagner, G., Neuhaus, D., Vašák, M., Kägi, J. H. R., and Wüthrich, K. (1985) *Eur. J. Biochem. 151*, 257−273.
47. Williamson, M. P., Havel, T. F., and Wüthrich, K. (1985) *J. Mol. Biol. 182*, 295−315.
48. Clore, M. G., Nilges, M., Sukumaran, D. K., Brunger, A. T., Karpus, M., and Gronenborn, A. M. (1986) *EMBO J. 5*, 2729−2735.
49. Wüthrich, K. (1986) *NMR of Proteins and Nucleic Acids*, John Wiley & Sons, New York.
50. Neuhaus, D., Wagner, G., Vašák, M., Kägi, J. R. C., and Wüthrich, K. (1984) *Eur. J. Biochem. 148*, 659−667.
51. Neuhaus, D., Wagner, G., Vašák, M., Kägi, J. R. C., and Wüthrich, K. (1985) *Eur. J. Biochem. 151*, 257−273.
52. Wagner, G., Neuhaus, D., Wörgötter, E., Vašák, M., Kägi, J. R. C., and Wüthrich, K. (1986) *Eur. J. Biochem. 157*, 257−289.
53. Nilges, M., Clore, G. M., and Gronenborn, A. M. (1988) *FEBS Lett. 229*, 317−324.
54. Arseniev, A., Schultze, P., Wörgötter, E., Braun, W., Wagner, G., Vašák, M., Kägi, J. H. R., and Wüthrich, K. (1988) *J. Mol. Biol. 201*, 637−657.
55. Henehan, C. J., Pountney, D. L., Zerbe, O., and Vašák, M. (1993) *Protein Sci. 2*, 1756−1764.
56. Braun, W., Vašák, M., Robbins, A. H., Stout, C. D., Wagner, G., Kägi, J. H. R., and Wüthrich, K. (1992) *Proc. Natl. Acad. Sci. U.S.A. 89*, 10124−10128.
57. Ejnik, J., Muñoz, A., Gan, T., Shaw, C. F., III, and Petering, D. H. (1999) *J. Biol. Inorg. Chem. 6*, 784−790.
58. Yu, X., Wu, Z., and Fenselau, C. (1995) *Biochemistry 34*, 3377−3385.
59. Antoine, M., Fabris, D., and Fenselau, C. (1998) *Drug Metab. Dispos. 26*, 921−926.
60. Wei, D., Fabris, D., and Fenselau, C. (1998) *Drug Metab. Dispos. 27*, 786−791.
61. Yu, X., Wu, Z., and Fenselau, C. (1995) *Biochemistry 34*, 3377−3385.
62. Zaia, J., Fabris, D., Wei, D., Karpel, R. L., and Fenselau, C. (1998) *Protein Sci. 7*, 2398−2404.
63. Krezoski, S. K., Villalobos, J., Shaw, C. F., III, and Petering D. H. (1988) *Biochem J. 255*, 483−491.
64. Petering, D. H., Quesada, A., Dughish, M., Krull, S., Gan, T., Lemkuil, D., Pattanaik, A., Byrnes, R. W., Savas, M., Whelan, H., and Shaw, C. F., III (1993) in *Metallothionein III: Biological Roles and Medical Implications* (Suzuki, K. T., Imura, N., and Kimura, M., Eds.) pp 329−346, Birkhäuser Verlag, Basel, Switzerland.
65. Klaassen, C. D., Liu, J., and Choudhuri, S. (1999) *Annu. Rev. Pharmacol. Toxicol. 39*, 267−94.
66. Misra, R. R., Hochadel, J. F., Smith, G. T., Cook, J. C., Waalkes, M. P., and Wink, D. A. (1996) *Chem. Res. Toxicol. 9*, 326−32.

BI0205956